doi:10.1246/cl.2011.773
Published on the web June 25, 2011


# Synergistic Cell Killing by Magnetic and Photoirradiation Effects of Neck-structured $\alpha$-$Fe_2O_3$ against Cancer (HeLa) Cells

Md. Shariful Islam,[1] Yoshihumi Kusumoto,*[1] Md. Abdulla-Al-Mamun,[1] and Yuji Horie[2]
[1]*Department of Chemistry and Bioscience, Graduate School of Science and Engineering, Kagoshima University, 1-21-35 Korimoto, Kagoshima 890-0065*
[2]*Department of Electrical and Electronics Engineering, Graduate School of Science and Engineering, Kagoshima University, 1-21-40 Korimoto, Kagoshima 890-0065*

(Received April 25, 2011; CL-110347; E-mail: kusumoto@sci.kagoshima-u.ac.jp)

Nanosized neck-structured $\alpha$-$Fe_2O_3$ nanoparticles were prepared successfully from iron(II) chloride tetrahydrate solely by hydrothermal method. FE-SEM and TEM studies revealed a unique necked structure with a particle size of ca. 50–60 nm. The synthesized nanomaterials showed excellent colloidal stability and magnetization ability. Finally, the as-prepared $\alpha$-$Fe_2O_3$ nanoparticle suspensions showed almost 100% cancer cell killing by the significant temperature increment when an AC (alternating current) magnetic field and photoirradiation were applied at a concentration of 80 $\mu g\,mL^{-1}$ MEM (minimum essential medium).

Iron oxides exist in nature in many forms in which magnetite ($Fe_3O_4$), maghemite ($\gamma$-$Fe_2O_3$), and hematite ($\alpha$-$Fe_2O_3$) are probably most common.[1] Hematite ($\alpha$-$Fe_2O_3$) is the oldest iron oxide and is widespread in rocks and soils. It is the most stable iron oxide under ambient conditions and has significant scientific and technological importance.[2] The stability and semiconductor properties of $\alpha$-$Fe_2O_3$ allow it to be used as a photocatalyst.[3] Currently $\alpha$-$Fe_2O_3$ photoelectrodes have received considerable attention as solar energy conversion material due to its excellent properties, such as a small band gap (2.1 eV), high resistivity to corrosion, and low cost.[4]

In an alternating current (AC) magnetic field, induced currents are generated in metallic objects, and as a consequence, heat is generated in the metal. This phenomenon is greatly enhanced in metals showing collective magnetic behavior. Thus, when a magnetic fluid is exposed to an AC magnetic field, the particles become powerful heat sources, destroying tumor cells since these cells are more sensitive to temperatures in excess of 41 °C than their normal counterparts.[5] Hyperthermia is a therapeutic procedure that promotes the increase of temperature in body tissues in order to change the functionality of the cellular structures. Its activity is based on the fact that a temperature increase to 41–42 °C can induce tumor cell death, as the tumor cells are less resistant to sudden increases in temperature than the normal surrounding cells.[6]

$\alpha$-$Fe_2O_3$ is a well-known semiconductor but cannot produce sufficient OH radicals under photoirradiation, and its low saturation magnetization value cannot produce enough heat for a hyperthermia level to kill cancer cells. In view of this, in this letter, we deal with the preparation and characterization of neck-structured $\alpha$-$Fe_2O_3$ nanoparticles and their successful utilization for thermal cancer cell killing under combined AC magnetic-field induction and visible light irradiation.

Typical syntheses of magnetite ($Fe_3O_4$) nanoparticles were carried out in a hydrothermal system. $FeCl_2 \cdot 4H_2O$ (0.99 g, 5 mmol) was dissolved in ethylene glycol (40 mL) to form a clear solution, followed by the addition of sodium acetate (anhydrous, 3.6 g) and poly(ethylene glycol) (1.0 g). The mixture was stirred vigorously for 45 min until getting a clear solution and then sealed in a Teflon-lined stainless-steel autoclave (50 mL capacity). The autoclave was heated to and maintained at 190 °C for 5 h and allowed to cool to room temperature. After cooling, decantation was done by a permanent magnet to get the sedimented black products. The black products were washed several times with ethanol and dried at 70 °C for 3 h. Finally, we obtained 0.81 g of $Fe_3O_4$ nanoparticles, and then the magnetite nanoparticles were oxidized to maghemite (data not shown) and hematite at 250 °C for 8 h in the presence of oxygen and at 500 °C for 3 h in the presence of Ar gas, respectively.[7] The prepared nanoparticles were characterized by using FE-SEM, TEM, XRD, and UV–vis absorption (reflectance) spectra. Colloidal stability was observed by dispersing the nanoparticles in distilled water using a permanent magnet, and magnetic hysteresis loops were measured by superconducting quantum interference devices (SQUID, Quantum Design MPMS-5).

HeLa cells were provided by the RIKEN BRC through the National Bio-Resource Project of the MEXT, Japan. The mentioned cancer cell line was cultured in a minimum essential medium (MEM) solution with 10% newborn calf serum (NBS) in a humidified incubator with an atmosphere of 5% $CO_2$ in air at 37 °C, and the cells were plated at a concentration of about $3 \times 10^5$ in 60 mm Petri dishes and allowed to grow for 3 days. Monolayer cultures of cancer cell line (HeLa Cells) were maintained as described by Abdulla-Al-Mamun et al.[8]

The in vitro cytotoxicity and anticancer effect of the as-prepared nanoparticles against the HeLa cell line were evaluated by Trypan Blue exclusion. In the experiment, an AC magnetic-field was created by using a magnetic oscillator with desired frequency and strength of 560 kHz and 5.0 $kA\,m^{-1}$, and a Xenon lamp (CERMAX 300-W LX300F, USA) with heat cut-off and band-pass filters (400–800 nm) with an average intensity of 30 $mW\,cm^{-2}$ was used for the light irradiation on HeLa cells. To investigate the cytotoxicity efficacy, every Petri dish was subjected to simultaneous AC magnetic-field induced and photoirradiated conditions for 5, 10, 15, 20, and 25 min with a dose of 80 $\mu g\,mL^{-1}$ of $\alpha$-$Fe_2O_3$ nanoparticles. Temperature increment for every dish was recorded by using a digital thermometer (Model SK-250WP II-R).

Particle morphology of the sample was studied using FE-SEM and TEM. Figure 1a represents the FE-SEM micrographs of neck-structured $\alpha$-$Fe_2O_3$, and the nanoparticles size was roughly estimated to be about 50–60 nm based on SEM and TEM data. Figures 1b, 1c, and 1d depict the TEM image, color,

  

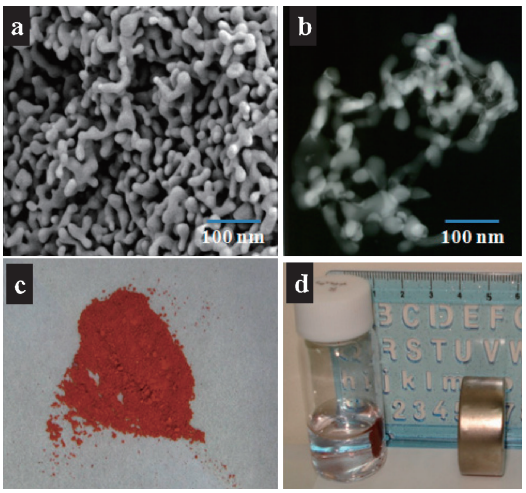


**Figure 1.** SEM (a), TEM (b) images, (c) color, and (d) colloidal stability of neck-structured $\alpha$-$Fe_2O_3$ nanoparticles.

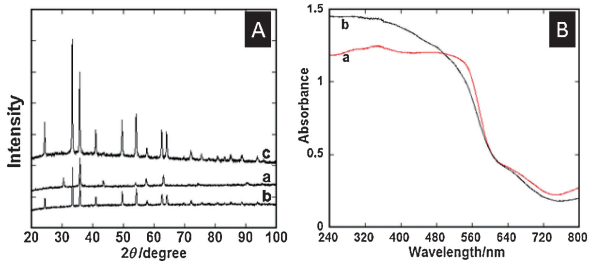


**Figure 2.** XRD patterns (A) and UV–vis absorption (reflectance) spectra (B) of neck-structured $\alpha$-$Fe_2O_3$ nanoparticles in comparison with commercial material; (a) $Fe_3O_4$ (mother sample), (b) commercial, and (c) as-prepared $\alpha$-$Fe_2O_3$ for plate (A) and (a) commercial and (b) as-prepared $\alpha$-$Fe_2O_3$ for plate (B).

and colloidal stability of $\alpha$-$Fe_2O_3$, respectively. The nanostructural homogeneities and remarkably unique neck-structured morphology were clearly observed by both FE-SEM and TEM. Such a unique morphology was observed for the first time in iron oxide with excellent magnetic properties.

To examine the colloidal stability of iron oxide samples, 10 mg of nanoparticles was dispersed in 50 mL of doubly distilled water by sonication. As shown in Figure 1d, lower, the as-prepared nanoparticles were well dispersed in water without any aggregation and precipitation and were firmly dragged by the permanent magnetic force, and the magnetic nanoparticles remained in suspension for more than 1 day, which demonstrates that they can be well-dispersed in aqueous solution.

The crystal structures and band gap of the prepared neck-structured hematite nanoparticles were observed by XRD and UV–vis absorption (reflectance) spectra. Typical XRD patterns and UV–vis absorption (reflectance) spectra of as-prepared and commercial (Wako, catalog No. 322-94283) $\alpha$-$Fe_2O_3$ are shown in Figure 2. The XRD pattern of $Fe_3O_4$ is shown in Figure 2A(a) which was transferred to $\alpha$-$Fe_2O_3$ (Figure 2A(c)), and it was clear that the diffraction peaks of as-prepared $\alpha$-$Fe_2O_3$ (Figure 2A(c)) were found to be consistent with the diffraction peak patterns of the commercial material (Figure 2A(b)). No

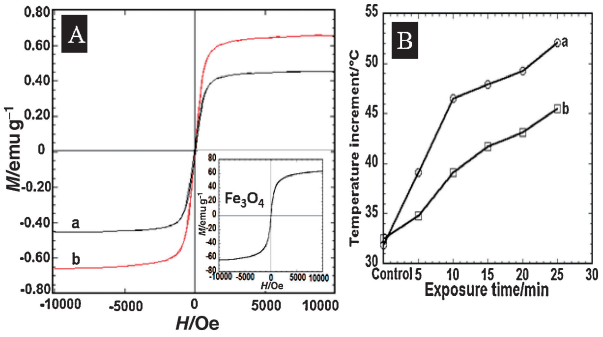


**Figure 3.** (A) Magnetic hysteresis loops of neck-structured $\alpha$-$Fe_2O_3$ nanoparticles (b) in comparison with commercial material (a) and $Fe_3O_4$ (inset). (B) Time dependent heat increment of $Fe_3O_4$ (a) and as-prepared $\alpha$-$Fe_2O_3$ (b) under combined AC magnetic-field induction and photoirradiation.

diffraction peaks from other crystalline forms are detected, which demonstrates that our prepared $\alpha$-$Fe_2O_3$ sample has high purity and crystallinity (JCPDS, PDF, File No. 01-089-0596). UV–vis spectroscopic studies were performed to ascertain the absorption edge of the as-prepared nanomaterials. Figures 2B(a) and 2B(b) represent the UV–visible diffuse reflectance spectra of commercial and as-prepared $\alpha$-$Fe_2O_3$, respectively. The absorption edge for both samples was at around 570–580 nm. The band gap estimated from the onset of the absorption edge was observed at 2.16–2.18 eV, which was in good agreement with a band gap value of 2.2 eV for $\alpha$-$Fe_2O_3$.[9]

Figure 3A shows the hysteresis loops of commercial (a) and as-prepared (b) $\alpha$-$Fe_2O_3$ and $Fe_3O_4$ (Figure 3A, inset) measured at room temperature. We noticed that the saturation magnetization values were 0.45, 0.67, and 65.8 emu $g^{-1}$, respectively, for commercial, $\alpha$-$Fe_2O_3$, and $Fe_3O_4$ nanoparticles, similar to the findings reported by Cornell et al.[1]

This is excellent evidence of the completion of the phase transformation of $Fe_3O_4$ to $\gamma$-$Fe_2O_3$ (data not shown) and $\alpha$-$Fe_2O_3$. Heat dissipation capability of $Fe_3O_4$ (Figure 3B(a)) and as-prepared $\alpha$-$Fe_2O_3$ (Figure 3B(b)) was evaluated by using an AC magnetic-field generator. The heat generated was evaluated with 80 μg $mL^{-1}$ magnetic nanoparticle suspension dispersed in MEM with exposing time 5, 10, 15, 20, and 25 min under both AC magnetic-field and photoirradiation conditions. The highest temperatures achieved were 52.1 and 45.5 °C for $Fe_3O_4$ and $\alpha$-$Fe_2O_3$, respectively, for 25 min exposure time whereas Ito et al. achieved 42.0 °C for 30 min exposure time using 100 μg $mL^{-1}$ concentration of magnetite nanoparticles under only AC magnetic field.[10] However, in this study we assumed that heat was generated through the combination of Brownian and Néel relaxation and magnetic hysteresis loss; to clarify it further detailed study is needed.

To evaluate the cytotoxicity, cell dishes were incubated for 24 h with 80 μg $mL^{-1}$ of $\alpha$-$Fe_2O_3$, and another dish without any nanoparticle solution (control dish) was also incubated for 24 h (Figure 4). The cancer cell viability under AC magnetic-field induced and photoirradiated conditions for exposure time 5, 10, 15, 20, and 25 min are shown in Figure 4.

We compared the heat increment and cytotoxicity of the same sample under three distinct conditions such as AC magnetic-field induction alone, photoirradiation alone, and

  

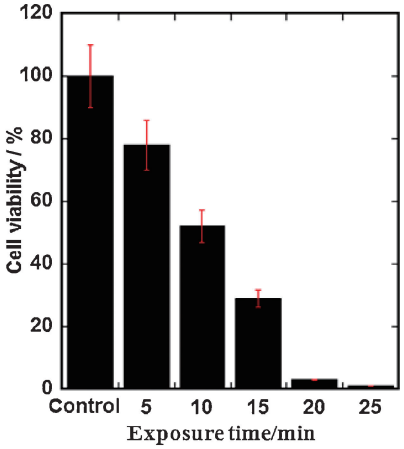


**Figure 4.** Time dependent cell viability using neck-structured $\alpha$-$Fe_2O_3$ nanoparticles under AC magnetic field and photo-irradiated conditions.

**Table 1.** Comparative heating and cell killing potentiality of neck-structured $\alpha$-$Fe_2O_3$ nanoparticles under different conditions

| | Exposure time/min | | | | | |
|---|---|---|---|---|---|---|
| | 20 | | | 25 | | |
| | $T_1$[a] | $T_2$[b] | $T_3$[c] | $T_1$[a] | $T_2$[b] | $T_3$[c] |
| Heat increment/°C | 39.3 | 37.1 | 43.1 | 40.2 | 38.5 | 45.5 |
| Cell viability/% | 77 | 86 | 3.1 | 58 | 76 | 0.5 |

[a]AC magnetic-field induction alone. [b]Photoirradiation alone. [c]AC magnetic-field induction + photoirradiation.

combined AC magnetic-field induction and photoirradiation with the same dose for 20 and 25 min (Table 1). The results revealed that highest temperature achieved was 45.5 °C along with almost 100% cells destruction under the combined AC magnetic-field induction and photoirradiation conditions ($T_3$) whereas for only AC magnetic-field induction ($T_1$) and only photoirradiated ($T_2$), temperature increment and cell destruction were 40.2 °C ($T_1$), 38.5 °C ($T_2$) and 42% ($T_1$) (viability: 58%), 24% ($T_2$) (viability: 76%), respectively, for 25 min exposure time. So, it can be clearly stated that under combined AC magnetic-field induction and photoirradiation for 25 min almost 100% of the cells were killed in the presence of 80 $\mu g\,mL^{-1}$ of $\alpha$-$Fe_2O_3$ (Figure 4).

Figure 5 shows microscopic images of HeLa cells. Figure 5a shows that the cell morphology is unchanged under simultaneous AC magnetic-field induced and photoexcited conditions without any nanoparticles. However, Figure 5b shows that the HeLa cells suffer severe thermal shock at 25 min exposure under the same conditions with $\alpha$-$Fe_2O_3$ nanoparticles. Finally, it can be concluded that increased exposure time increased heat increment and thus, increased cancer cell killing efficiency.

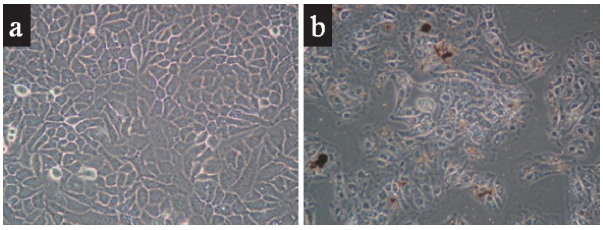


**Figure 5.** Microscopic images of HeLa cells (Magnification 200). (a) Control and (b) 25 min exposure under both AC magnetic field and photoirradiated conditions.

To the best of our knowledge, we synthesized for the first time $\alpha$-$Fe_2O_3$ nanoparticles of neck-structured shape with excellent colloidal stability and magnetic properties. This is the first report using $\alpha$-$Fe_2O_3$ nanoparticles for cancer cell killing under combined AC magnetic-field induced and photo-irradiated conditions.

The present work was partly supported by Grant-in-Aid for Scientific Research (B) (No. 19360367) from Japan Society for the Promotion of Science (JSPS) and Grant-in-Aid for JSPS Fellows (No. 22·00083).

## References

1 R. M. Cornell, U. Schwertmann, *The Iron Oxides: Structure, Properties, Reactions, Occurrences and Uses*, 2nd ed., Wiley-VCH, Weinheim, **2003**.
2 R. Dieckmann, *Philos. Mag. A* **1993**, *68*, 725.
3 H. H. Kung, *Transition Metal Oxides: Surface Chemistry and Catalysis*, Elsevier, New York, **1989**.
4 T. Ohmori, H. Takahashi, H. Mametsuka, E. Suzuki, *Phys. Chem. Chem. Phys.* **2000**, *2*, 3519.
5 A.-H. Lu, E. L. Salabas, F. Schüth, *Angew. Chem., Int. Ed.* **2007**, *46*, 1222.
6 R. Cavaliere, E. C. Ciocatto, B. C. Giovanella, C. Heidelberger, R. O. Johnson, M. Margottini, B. Mondovi, G. Moricca, A. Rossi-Fanelli, *Cancer* **1967**, *20*, 1351.
7 S. Sun, H. Zeng, D. B. Robinson, S. Raoux, P. M. Rice, S. X. Wang, G. Li, *J. Am. Chem. Soc.* **2004**, *126*, 273.
8 M. Abdulla-Al-Mamun, Y. Kusumoto, A. Mihata, M. S. Islam, B. Ahmmad, *Photochem. Photobiol. Sci.* **2009**, *8*, 1125.
9 W. B. Ingler, Jr., S. U. M. Khan, *Int. J. Hydrogen Energy* **2005**, *30*, 821.
10 A. Ito, M. Shinkai, H. Honda, K. Yoshikawa, S. Saga, T. Wakabayashi, J. Yoshida, T. Kobayashi, *Cancer Immunol. Immunother.* **2003**, *52*, 80.

  